Mine Water and the Environment (2019) 38:252–260
https://doi.org/10.1007/s10230-019-00599-0

TECHNICAL ARTICLE

Evolution of Floor Water Inrush from a Structural Fractured Zone with Confined Water

Yanbo Hu[1] · Wenping Li[1] · Qiqing Wang[1] · Shiliang Liu[1] · Zhenkang Wang[1]

Received: 15 May 2018 / Accepted: 26 February 2019 / Published online: 4 March 2019

Abstract

Due to a gradual increase in mining depths in northern China, the water inrush problem there has become increasingly complex. In the present study, a physical model was developed of a syncline-axis structural fractured zone above confined water, using measured parameters from the Baizhuang coal mine. Using the similarity theory, water inrush from a fractured floor was simulated with different water heads and different structural zones. The mechanism of a delayed water inrush from the floor under the combined action of confined water and a fractured zone was also studied. The results demonstrated that: (1) Water inflow under different pressures; (2) Sand inrush discharges gradually increased under various pressurized water pressures and then decreased; and (3) Based on water and sand inrush discharges, the changes in the Reynolds number and porosity were analyzed, and a "void flow-fissured flow-pipeline flow" transition was proposed. This research provides a basis for developing methods to prevent floor water inrush during deep mining.

Keywords Void flow · Fissured flow · Pipeline flow

Introduction

In recent years, there has been a significant increase in coal mining depths in northern China. Consequently, water inrush events have occurred from a lower coal group due to structural fractures of the mining area (Guo et al. 2018; Zhang et al. 2015). Statistics show that during mining, water inrush from the hidden floor structure makes up more than half of the total water inrush (Hu 2017). In particular, floor water inrush events associated with large percolation channels occur more frequently in northern China, where the percolation channels are expanded by water flow in the structurally fractured zone. Consequently, the water inrush problem is made more complicated by this fractured zone and the high water pressure (Caine et al. 1996; Huang et al. 2018).

Although few scholars have studied the mechanism of water inrush from coal seam floor under the coupled action of high pressure water in a fractured zone, a great deal of relevant research has been done. The "strong percolation channel" theory proposed by the Institute of Geology and Geophysics of the Chinese Academy of Sciences states that the water inrush channel is the key factor in a floor water inrush. The channels include intrinsic and secondary channels formed by various geological factors. This theory focuses on the effect of geological structure factors on water inrush (Ren and Shan 2014; Shi 2009). Pradip and Venkataraman (1995) studied the non-Darcian converging flow velocities of a coarse-grained fractured rock mass; their experimental results demonstrated that the percolation behavior of a fractured rock mass obeyed the Missbach and Forchheimer equations. Legrand (2002) studied the effect of water pressure on seepage during percolation through fractured rock with a large number of similarity tests. Wu et al. (2002) put forward the new concept of a water inrush time lag effect caused by fault structures *i* obtained the effect of water pressure on seepage *n* the coal seam floor through an in-situ stress measurement method, uniaxial and triaxial compression testing, as well as rheological mechanics testing under different water content conditions. Wu et al. (2007a) studied the water blocking strength of a rock mass in the fault zone

Electronic supplementary material The online version of this article (https://doi.org/10.1007/s10230-019-00599-0) contains supplementary material, which is available to authorized users.

✉ Wenping Li
wplicumt@126.com

[1] School of Resources and Geosciences, China University of Mining and Technology, Xuzhou, Jiangsu 221116, China

and found that it was less than in an intact rock stratum. Ma et al. (2009) studied the percolation characteristics of fractured sandstone and shale with different particle sizes and under different stress levels, and obtained the relationship between axial stress and permeability. Prof. Li Wenping performed a physical mechanics experimental study on the floor of a working face with optical fiber and grating, and determined the relationship between the constituent materials in the structural fractured zone and the confining pressure, as well as the characteristics of load action and height of the water head of the aquifer.

In addition, in situ tests of the water resistance of a rock mass were performed in the structural fracture zone, and the mechanism conditions and prevention theory were proposed for a lagging water inrush formed by the joint action of pressurized water and mining pressure in a structural fracture zone (Qiao and Li 2011). Through lateral pressure testing, particle migration experiments have been carried out during water inrush under high pressure; the results indicated that the evolution of permeability in a granular sandstone during a highly-pressurized floor water inrush could be divided into four stages (Bai et al. 2013; Ma et al. 2016). In the present study, a physical model was developed of a water inrush occurrence in the syncline-axis structural fracture zone above confined water, using the Baizhuang coal mine as an example. Then the variation rules of water inflow and sand volume during water inrush were simulated under different water pressures and different structural fracture zones and the effects of the Reynolds number rules and porosity on water inrush were further analyzed. The results can provide a theoretical basis for the early warning and prevention of water inrush that occurs due to high pressure water in a tectonic fracture zone.

Research area

The Baizhuang coal mine is located in the mid-western part of the Feicheng coal field. Administratively, it belongs to the territory of Hutun Town in Feicheng City (Fig. 1). The geographic coordinates are: longitude − 116°34′46″–116°38′20″E and latitude − 36°13′25″–36°16′11″N. The folds in the Baizhuang coal mine are mainly controlled by large fractures. Several irregular folds occur near the large fractures or between large- and medium-sized fractures. These are characterized by asymmetry and possess the characteristics of a short-axis. Actual mining data for the 7th coal seam demonstrated that a syncline structure with a NE axial direction existed in the middle of the 4th and 6th mining areas at the 150 m level of the well field. The amplitude and width of the syncline structure were relatively low and the inclination angles of the two wings generally ranged within 3–8°. The actual mining data of the 8th and 9th coal seams

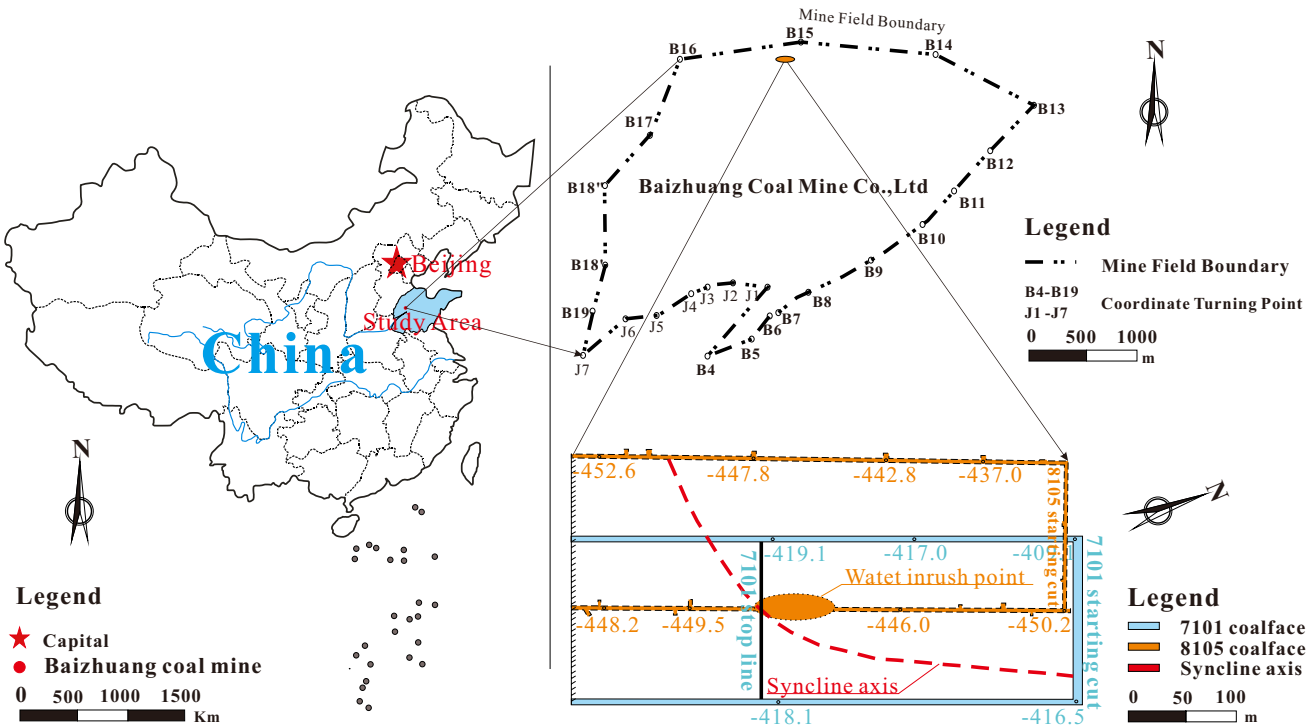

Fig. 1 Geographical location diagram

demonstrated that the axial part of syncline developed into a group of echelon reverse fault fracture zones; the height of the 7101 working face of Baizhuang coal mine ranged from −432.2 to −391.6 m and the face length ranged from 60 to 123 m, with a recoverable reserve of 199,000 tons. The working face was located at the south wing of syncline axis and the syncline axis rose to the NE. The coal rock strata on the south wing of syncline axis had a strike angle between 57° and 80° and an inclination between 327° and 350°. Within the recovery range, the dip angle of the coal strata was relatively low, between 2° and 6°. The maximum water inrush coefficient of the 5th thin limestone layer at the 7101 working face was 0.049 MPa/m, while the maximum value of the Ordovician limestone was 0.059 MPa/m.

Recovery of the working face began on Oct 25th, 2015. On Jan 11th, 2016, mining was terminated due to the poor coal quality; the corresponding mining length was 230 m. At 4:15 am on Jan 25th, 2016 (14 days after mining stopped), the floor Ordovician water inrush occurred at the 8105 track entry beneath the terminal line. The 8105 working face was not being mined while the auxiliary roadway was being completed (Fig. 2). The maximum water discharge was measured to be 2800 m^3/h and the water inrush underwent three stages (Fig. 3). The first stage was from 04:15 to 08:00, lasting for approximately 4 h. During this stage, the floor water discharge was less than 200 m^3/h. The second stage was from 8:00 to 14:00, and the floor water discharge rapidly increased, from 400 to 2400 m^3/h, indicating that the moderate water inrush point evolved into a large water inrush point. The third stage was from 14:00 to 22:50, lasting for ≈8 h. The inrush discharge continued to increase rapidly, to ≈2800 m^3/h, clearly a very large water inrush point.

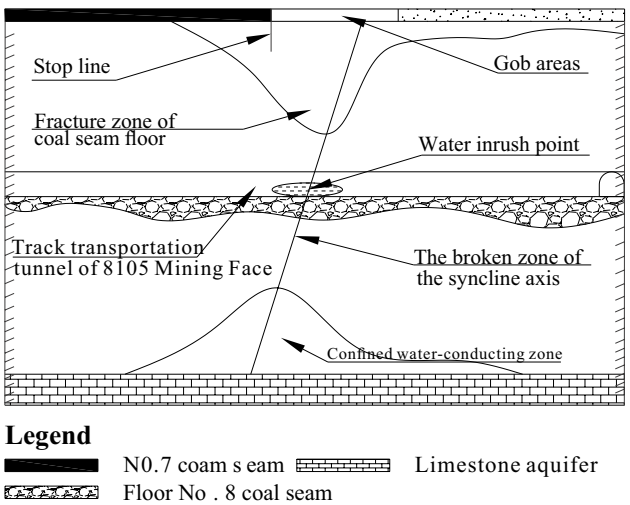

Fig. 2 Position of water inrush point

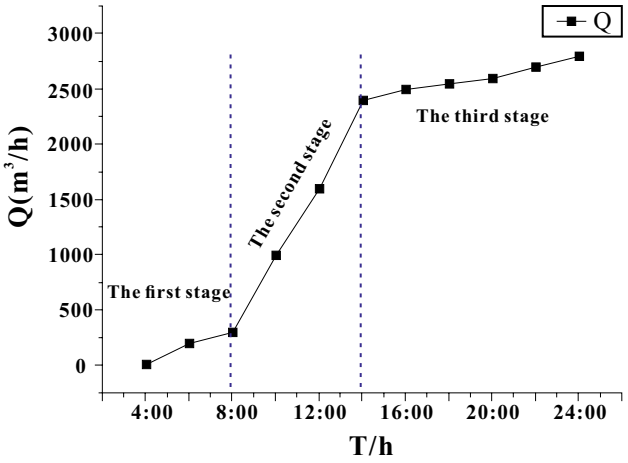

Fig. 3 Variation of water discharge during water inrush occurrence at Baizhuang coal mine

Similar Tests for Water Inrush in the Structural Fracture Zone

Analysis of Prototype During Simulation

The syncline-axis structural fractured zone in the seam floor of the 7101 working face of the Baizhuang coal mine (discussed above and presented in Fig. 1) is composed of conglomerate, mudstone, and coal powder, and was used as a prototype in the model test (Fig. 4).

According to the on-site mined rock of the concealed syncline-axis fractured zone exposed by the transportation tunnel of the 8105 mining face, and the floor borehole data of the 7101 working face, the fractured zone mainly comprised shale and mudstone. Parameters such as density, water content, uniaxial compressive strength, granularity distribution, and mineral composition of the rock (shale) were measured using rock samples (Liu 2017). The volume ratio of the conglomerate and mudstone was ≈3:2 in the fractured zone.

The core part width of the syncline-axis fracture zone was 10–20 m and no water existed when the fractured zone was revealed in the transportation tunnel of the 8105 mining face, indicating that the syncline-axis fractured zone did not originally contain water. Due to the effects of mining pressure, the confined water of the roadway floor exerted pressure on the fracture zone, resulting in seepage.

Design Model Experimental Equipment

The borehole near the 7101 working face revealed that the 7th seam was 77 m from the Ordovician limestone. The distance from the water inrush point to the Ordovician limestone in the transportation tunnel was 47 m (the inrush point in the transportation tunnel was located directly below where

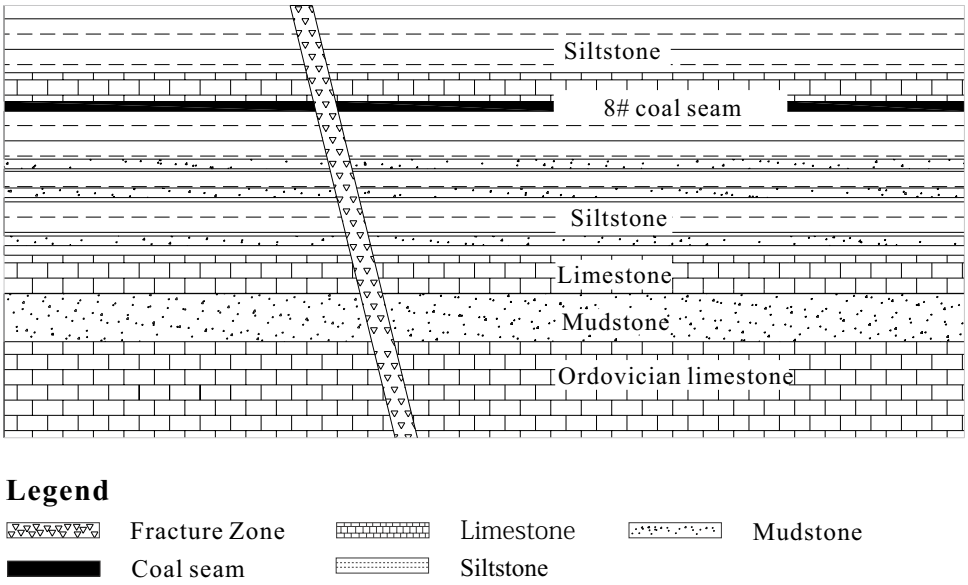

Fig. 4 Prototype stratigraphic sketch map of model test

the 7101 working face stopped). The Ordovician limestone water level was 24.6 m and its water pressure was 5.2 MPa. The model was designed using the geometric proportion of 1:100 (Fig. 5). The physical model for the concealed syncline-axis structure under high pressure had two parts: the dynamic pressurization equipment, a TX-800 high pressure mud pump, representing the confined water channel and cylindrical equipment simulating the water inrush channel.

According to similarity theory, the ratio of the model size to all dimensionless physical quantities must equal that of the prototype size to the same dimensionless physical quantities (Chui 1990; Wu et al. 2007b). The parameters of the on-site extracted sample from the fracture zone at the 7101 working face were simulated in the model of the water inrush channel (where H_1, H_2, H_3, and H_6 were 1640, 200, 20, and 200 mm, respectively).

The separation equipment for the particles flowing from the fractured zone consisted of two layers of a filter mesh. The first layer of filter mesh had a pore diameter of 2 mm, which allowed sand to pass through; the second layer of filter mesh had a pore size of 0.075 mm, which allowed muddy matter to pass through (according to GBJ145-90, the particle size of sand: $2 \geq d \geq 0.075$ mm and the particle size of a clay particle: $d \leq 0.075$ mm; Nanjing Hydraulic Research Institute 2008).

The rated maximal pressure of the high-pressure mud pump was 30 MPa, while the rated power and current were 300 KW and 3 A, respectively. The pipeline diameter was 110 mm. A pressure gauge (ranging from 0 to 15 MPa) and a high pressure switch (maximum pressure resistance of 32 MPa) were installed between the water-feed pipeline and the pump.

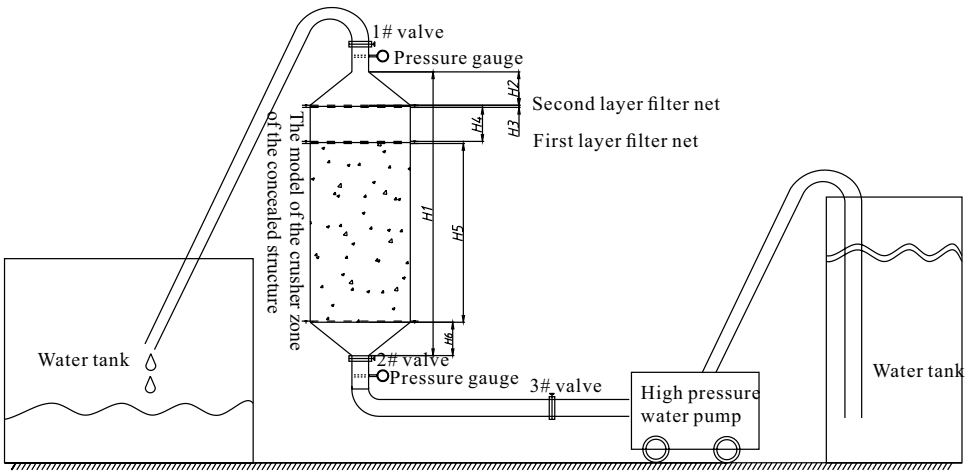

Fig. 5 Model map of concealed water inrush from high pressure water

The Experimental Scheme

The water inrush occurrence in the syncline-axis fractured zone simulated by the model was that as the 7101 coalface advanced, the effective floor aquitard thickness decreased due to the failure depth of the floor and the uplift of the Ordovician limestone confined water. Mining stopped when the mining face moved near the fracture zone; the water inrush then occurred 14 days later (Fig. 2).

The high pressure pump was used to simulate the pressure imposed by the Ordovician aquifer. The water inrush flow was measured while the pressure was gradually increased from 1.5 to 5.5 MPa.

The fill materials were composed of clay, coarse sand, and gravel in proportion to the particle size of the components in the syncline-axis structural fractured zone (Table 1), and they were mixed to fill the simulation device (Fig. 5).

Model I was used to simulate the syncline-axis fractured zone in the 7101 working face floor. The volume ratios of clay, coarse sand, and gravel were 1:1:3, to represent a loosely-filled, structural fractured zone.

Model II: The volume ratios of clay, coarse sand, and gravel in the simulated fractured zone were 2:1:2. The concealed water channel was 50% filled with the larger particles and 50% with clay particles, to represent a more densely filled structural fractured zone.

Model III: The volume ratios of clay, coarse sand, and gravel in the simulated fractured zone were 7:2:1, to represent a structural fractured zone with a clay skeleton.

The Experimental Procedure

First, the gravel, coarse sand, and clay were mixed in the same proportion as in the syncline-axis structural fractured zone to simulate the real syncline-axis structural fractured zone. Then they were put into the simulation device and compacted.

Second, the 1# valve was closed to add water to the simulation device with a water pump until the preset pressure was reached. Then the 1# valve was opened to measure the amount of outburst water at the constant pressure. The amounts of coarse sand and clay accompanying the water were also measured.

Table 1 Formulation of filling materials for the simulated syncline-axis fracture zone

Model	Volume of pebbles (m^3)	Volume of coarse sand (m^3)	Volume of clay (m^3)
I	0.0099	0.0033	0.0033
II	0.007	0.0035	0.007
III	0.0016	0.0032	0.0112

Third, the proportions were adjusted according to the orthogonal test table (Table 2), and then the process was repeated. Table 2 presents the different water pressures (1.5, 3.5, and 5.5 MPa), the three factors, and the three levels $L_9(3^3)$.

Results and Discussion

Changes in Discharge with Time

Figure 6 and supplemental Figures S-1 and S-2 present the changes in water inrush discharge, as simulated by the three models and different hydraulic pressures. The *q*-t curves indicate that:

1. During the initial stage of water inrush, the discharge was relatively low. With the continuous scouring and diameter-expansion actions on the syncline-axis fracture zone by the confined water, water flow began to increase. When the mud and sand were washed away from the

Table 2 Orthogonal table for testing

Test number	Water inrush pressure (MPa)	Properties of concealed structural fracture zone
1	1.5	Model I
2	3.5	Model I
3	5.5	Model I
4	1.5	Model II
5	3.5	Model II
6	5.5	Model II
7	1.5	Model III
8	3.5	Model III
9	5.5	Model III

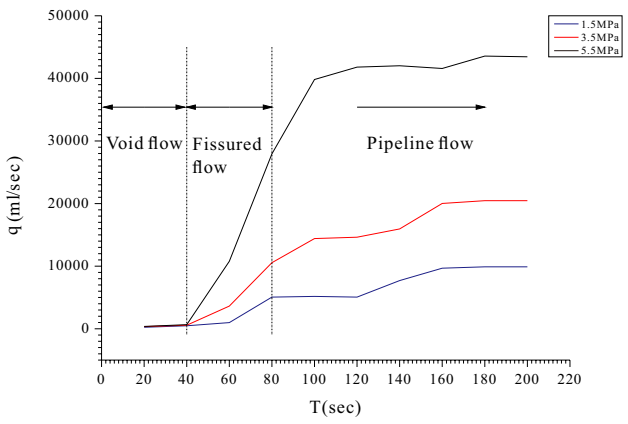

Fig. 6 Curves of water inrush and action time under different pressures for model I

fractured zone, the inrush channel no longer changed significantly, which caused the water inrush volume to stabilize.

2. In the curve of water flow vs. time, the corresponding time point of every increase in water inflow was the time of the change in the inflow channel. At different pressures, the models had different developmental points, corresponding to the transition from small pores to small fractures and from small fractures to larger fractures. The transition (inflection) points for Model I, at a pressure of 1.5 MPa, was at 60 and 120 s, while they were at 40 and 100 s at a pressure of 3.5 and 5.5 MPa. For Model II and Model III, the transition points were at 80 and 120 s at 1.5 MPa, 80 and 100 s at 3.5 MPa, and 60 and 80 s at 5.5 MPa.

Simultaneously, the water inrush discharge increased as the water pressure increased. Also, as the water pressure increased, the transition time among the three channel types significantly decreased. The time corresponding to the inflection points on the curve was the time when the water inrush mode changed, reflecting the gradual change of the flow channel from a small void to a fracture and then to a fissure.

Variations in Range of Sand Spring

Figure 7 and supplemental Figures S-3 and S-4 present the curves for the range of sand discharged, given by the three models at different pressures. The graphs show that:

1. At a certain period, the range of sand discharged increased, and then decreased, representing a peak on a curve. The occurred because the continuous scouring during the inrush caused the clay and sand content to gradually decrease.
2. As the water pressure increased, the sand inrush increased, and the time for the peak to be reached was shorter, because the higher pressure led to both stronger scouring ability and higher scouring speed. However, at a water pressure of 3.5 MPa, the sand volume of model II reached its peak value first (supplemental Figure S-3), because the ratio of clay, coarse sand, and gravel in model II is 2:1:2. In seepage from a fractured rock mass, there is a phenomenon of seepage attenuation due to an uneven distribution of permeability. That is to say, under the action of water pressure in the experimental device, small particles may accumulate at the top of the column, leading to velocity attenuation, and less permeability and starting pressure gradient at the top of the experimental device. At the material parameter ratio of model II, the accumulation velocity of small particles at a water pressure of 5.5 MPa water pressure was greater, which caused the decreased permeability. Therefore, the peak value of Q at 5.5 MPa fell behind that of Q at 3.5 MPa.

Analysis of the Reynolds Number

According to percolation dynamics, as the Reynolds number (*Re*) increases, the flow state in porous media (sand layer) undergoes three stages: (1) A linear laminar flow stage with an approximate upper limit of *Re* =10; the viscous force is dominant and Darcy's law applies to this stage. (2) A non-linear laminar flow zone (transition zone); the laminar flow is mainly restricted by inertial force and Darcy's law does not apply. The transition from laminar to turbulent flow occurs around the upper limit, *Re* = 100. (3) A turbulent flow stage: inertial force dominates and Darcy's law does not apply (Burger et al. 2015; Huang 2012; Niebling et al. 2012).

As presented in Fig. 8 and supplemental Figures S-5 ansd S-6, the water inrush discharge gradually increased within

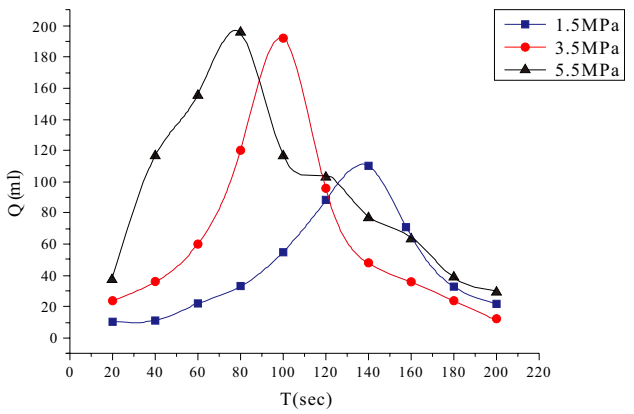

Fig. 7 Curves of sand bursting and action time under different pressures for model I

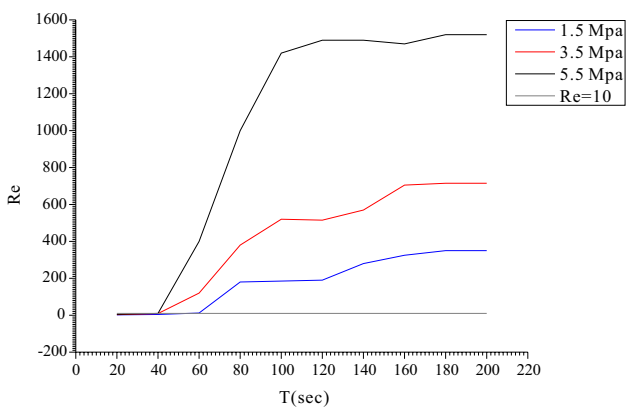

Fig. 8 Curves of Reynolds number and action time under different pressures for model I

the same time interval. As the permeation coefficient of the fill materials changed, the percolation discharge increase led to a greater discharge and an increase in the Reynolds number. As large amounts of mud and sand were discharged, the water inrush channel's porosity increased, resulting in a rapid increase of *Re* (*Re* > 10). The percolation flow state no longer obeyed Darcy's Law for a porous medium, and the transition in flow state occurred (Liu et al. 2007; Wu et al. 2003).

Then, the model was used as an example to calculate *Re*, using the obtained experimental data, and the variation in *Re* was used to analyze the percolation state transition during water inrush.

$$Re = \frac{\rho v d}{\mu} \tag{1}$$

$$v = \frac{Q}{T} \tag{2}$$

$$Re = \frac{\rho Q d}{T \mu} \tag{3}$$

where v is the characteristic velocity of the flow field, d is a characteristic length, and μ is the dynamic viscosity coefficient of water flow, which is related to temperature. When the water temperature was 15 °C, $\mu = 0.01$ cm^2/s.

The Reynolds numbers were calculated according to Eq. (3) and the Re curves given by the three models under different pressures were plotted (Fig. 8 and supplemental Figures S-5 and S-6).

1. During the tests, all three models had a laminar flow stage during the initial stage of water inrush, obeying Darcy's law (at $Re \leq 10$). For model I, Darcy flow occurred within 0–20 s at 1.5 and 3.5 MPa. For model II, it occurred within 0–40 s at 1.5 and 3.5 MPa, and within 0–20 s at 5.5 MPa; for model III, it occurred within 0–80 s under 1.5 MPa and 3.5 MPa, along with within 0–60 s under 5.5 MPa. Only when the water inrush pressure of model I was 5.5 MPa was the initial state a non-Darcy flow. The reason was that when the water inrush pressure was high, the clay, the sand and the other fine-grained materials were rapidly extracted, resulting in a relatively clear channel and a very short Darcy flow period. However, since the discharge was counted every 20 s, the transient Darcy flow stage was not observed.
2. During the water inrush experiment, there were two obvious time points of sudden increase in Reynolds number curves at a certain water pressure: 40 and 120 s at 1.5 MPa, 40 and 100 s at 3.5 and 5.5 MPa (Fig. 8); 80 and 100 s at 1.5 and 3.5 MPa, 60 and 80 s at 5.5 MPa (supplemental Figure S-5); and 80 and 120 s at 1.5 and 3.5 MPa, and 80 and 140 s at 5.5 MPa (supplemental Figure S-6).
3. As the water inrush pressure increased from 1.5 to 5.5 MPa, the duration of the Darcy flow ($Re \leq 10$) was rapidly shortened, while the *Re* within the same time interval increased. Moreover, when $Re \leq 10$, the Re increased slowly, but when $Re > 10$, it increased rapidly. The inflection points on the curve as the Re increased represented the points where the percolation mode changed (void flow to fissured flow to pipeline flow) during the water inrush.

Variations in Porosity

The porosity was calculated from the original experimental data and the changes in porosity were used to analyze the transition law for the percolation mode during water inrush (Milan and Andjelko 1992; Wang 2014). The calculation equations for porosity were:

$$n = \frac{v_s}{v_d} \tag{4}$$

$$v_d = \frac{\pi d^2 \left(h_1 - h_2 - h_3 - h_4 - h_6\right)}{4} \tag{5}$$

$$v_s = v_d - v_\rho \tag{6}$$

$$v_\rho = \frac{m - m_t}{\rho_\vartheta} \tag{7}$$

$$n_t = \left[\frac{\pi d^2 \left(h_1 - h_2 - h_3 - h_4 - h_6\right)}{4} - \frac{m - m_t}{\rho_\vartheta}\right] \Big/ \left[\frac{\pi d^2 \left(h_1 - h_2 - h_3 - h_4 - h_6\right)}{4}\right] \tag{8}$$

where v_s—volume of pores; v_d—total volume of material in experimental container; d—diameter of cylindrical percolation channel, with a selected value of 200 mm; h_1, h_2, h_3, h_6—constant values; h_4, h_5—dependent variables; m—mass of filling materials in fracture zone prior to pressurization; m_t—filling material scoured in unit interval following pressurization; ρ_ϑ—average density of filling materials; v_ρ—the volume of sand and gravel rushed out; and n_t—the porosity at unit time point.

The porosity variation curves (Fig. 9 and supplemental Figures S-7 and S-8) given by the three water inrush models indicate that:

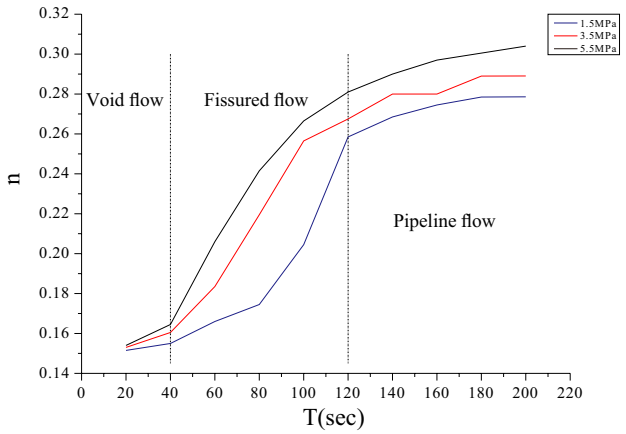

Fig. 9 Curves of porosity and action time under different pressures of model I

1. Due to continuous scouring by the confined water, the micro-fractures or voids in the cylindrical body of the syncline-axis fracture zone were expanded as fine-grained materials, such as mud and sand, were extracted from the cylinder. This was also expressed by the way fractures transited into channels, as porosity increased. As presented in Fig. 9 and supplemental Figures S-7 and S-8, the changes in porosity within 40 s were smoother and the porosity itself was less; the porosity continuously increased during the following 80 s; after 120 s, the porosity tended to stabilize, which was the main characteristic of the pipeline flow stage. The overall trends of models II and III were similar to that of model I, except for the variation times and porosity values.
2. As the clay and sand were extracted from the fractured zone, the inrush channels in the cylindrical body grew. The changes in porosity was similar to the changes in the Reynolds number and water inrush discharge, i.e. the porosity continuously increased along with the water pressure. The porosity increase changed the permeability coefficient and ultimately affected the changes in both flow state and percolation mode.

Thus, the composition variation of the filling material in the structural fracture zone was fundamental to the changes in the inrush discharge and the percolation mode. The porosity trends and the inflection points reflected the physical conditions of the three channel types, namely the void flow, fissured flow, and pipeline flow.

Conclusions

Using measured parameters from the prototype mine and applying similarity theory, the floor water inrush in the syncline-axis structural fractured zone was simulated at head pressures of different heights with different structural zone properties. The following conclusions were drawn:

1. The amount of water inrush from the transportation tunnel of the 8105 coal face in Bai Zhuang coal mine underwent three stages, from small to large as the water inrush in the fractured zone of the roadway floor went from void flow to fissure flow, and then to pipeline flow. This progressive transformation turned a water inflow into a disaster.
2. The sand emission volume in the discharge went from small to large to small with time. As the small particles were gradually eroded away, the cracks were scoured, increasing the fissure apertures and changing the nature of the channel.
3. According to the test results for Models I-III, laminar flow existed in the initial water inrush for all three models. During this period, all flows fit Darcy's law (Reynolds number ≤ 10). It was observed that the Reynolds number increased at two apparent inflection points during the entire water inrush. The experimental research demonstrated that the changes in porosity and the positions of the inflection points reflected the physical conditions of void flow, fissure flow, and pipeline flow.

The water inrush from the floor syncline fracture zone in the 8105 working face was experimentally simulated. The results show that the process of water inrush from the floor of a structural fracture zone in the mining face transitioned from void flow to fissure flow, and then to pipeline flow. The mechanism of delayed water inrush from the floor of a structural fractured zone in the mining face accurately predicted the specific transition from seepage to inrush. At the same time, combined with a dynamic system to monitor how the floor water flow is changing, it can be used to provide effective early warning in different stages of floor water inrush under similar conditions. The research results provide a strong basis for preventing and controlling floor water inrush events from the lower coal seam above the confined water level in northern China.

Acknowledgements This work was supported by the National Basic Research Program of China (973 Program) under Grant 2015CB251601, and the State Key Program of the National Natural Science Foundation of China under Grant 41430643.

References

Bai H, Ma D, Chen Z (2013) Mechanical behavior of groundwater seepage in karst collapse pillars. Eng Geol 164:101–106

Burger JH, Haldenwang R, Chhabra RP, Alderman NJ (2015) Power law and composite power law friction factor correlations for laminar and turbulent non-Newtonian open channel flow. J Braz Soc Mech Sci 37(2):601–612

Caine JS, Evans JP, Forster CB (1996) Fault zone architecture and permeability structure. Geology 24(11):1025–1028

Chui GX (1990) Similarity theory and model test. China Univ of Mining and Technology Press, Xuzhou

Guo WJ, Zhang SC, Sun WB, Chen JT (2018) Experimental and analysis research on water inrush catastrophe mode from coal seam floor in deep mining. J Chin Coal Soc 43(01):219–227

Hu Y (2017) Mining effect and influencing factors of fault activation water inrush above confined aquifers. PhD diss, AnHui Univ of Science & Technology

Huang K (2012) Exploration of the basic seepage equation in porous media. PhD Diss, China Univ of Geosciences, Wuhan

Huang GS, Zhai XX, Tu XZ, Li RB, Zhang SW (2018) Research on seam floor failure depth in coal mining above aquifer under different conditions. Coal Eng 50(2):95–99

Legrand J (2002) Revisited analysis of pressure drop in flow through crushed rocks. J Hydraul Eng 128(11):1027–1031

Liu P (2017) Experimental and numerical simulating studies on hydrofracturing mechanism of glutenite. PhD diss. China Univ of Mining & Technology, Beijing

Liu QM, Li WP, Zeng XG, Jiang GL, Zhao LT (2007) Indoor hydraulic pressure cracking method to test and measure critical breaking pressure and water resistance coefficient of rock mass. Coal Sci Technol 35(1):85–87

Ma ZG, Miao XX, Chen ZQ, Li YS (2009) Experimental study of permeability of broken coal. Rock Soil Mech 30(4):985–988

Ma D, Rezania M, Yu HS, Bai HB (2016) Variations of hydraulic properties of granular sandstones during water inrush: effect of small particle migration. Eng Geol 217:61–70

Milan V, Andjelko S (1992) Determination of hydraulic conductivity of porous media from grain-size composition **(No. 551.49 V 986)**

Nanjing Hydraulic Research Institute (2008) Standard for engineering classification of soil. China Planning Press, Xuzhou

Niebling MJ, Toussaint R, Flekkøy EG, Måløy KJ (2012) Dynamic aerofracture of dense granular packings. Phys Rev E 86(6):061315

Pradip KGN, Venkataraman P (1995) Non-Darcy converging flow through coarse granular media. J Inst Eng Civil Eng 504(76):6–11

Qiao W, Li WP (2011) Effect of geo-stress on permeability of groundwater in karst-fractured rock mass. J China Univ Min Tech 40(1):73–79

Ren YH, Shan BJ (2014) Safety Evaluation and numerical simulation of 16# coal seam mining above confined water in Pinggou Coal Mine. Coal Technol (12): 188–191

Shi LQ (2009) Summary of research on mechanism of water-inrush from seam floor. J Shandong U Sci Tech 28(3):17–23

Wang LZ (2014) Accelerated Experimental Study on Permeability for Broken Mudstone with Mass. PhD diss. China U Min Tech, Xuzhou

Wu Q, Liu JT, Zhong YP, Yin ZR, Li JM, Hong YQ, Ye GJ, Tong YD, Dong DL (2002) The numeric simulations of water-bursting time-effect for faults in Zhaogezhuang coal mine, Kailuan, China. J Chin Coal Soc 27(5):511–516

Wu Q, Zhou YJ, Liu JT, Zhong YP, Yin ZR, Li JM, Hong YQ, Zhou RG (2003) The mechanical experiment study on lag mechanism of water-bursting of fault under coal seam. J Chin Coal Soc 28(6):561–565

Wu JW, Tong HS, Tong SJ, Tang DQ (2007a) Study on similar material for simulation of mining effect of rock mass at fault zone. Chin J Rock Mech Eng (S2):4170–4175

Wu FF, Cao P, Wan LH (2007b) Similarity theory and its application in simulation test. Min Technol 7(4):64–65

Zhang SC, Guo WJ, Sun WB, Li YY, Wang HL (2015) Experimental research on extended activation and water inrush of concealed structure in deep mining. Rock Soil Mech 36(11):3111–3120